Available online at www.sciencedirect.com

ScienceDirect

IFAC PapersOnline CONFERENCE PAPER ARCHIVE

IFAC PapersOnLine 55-31 (2022) 91–97

Hybrid Tracking Controller for an ASV Providing Mission Support for an AUV

Torbjørn R. Fyrvik * **Jens E. Bremnes** * **Asgeir J. Sørensen** *

* *Centre for Autonomous Marine Operations and Systems (AMOS), Department of Marine Technology, Norwegian University of Science and Technology (NTNU), Otto Nielsens veg 10, 7491 Trondheim, Norway (e-mails: torbjofy@stud.ntnu.no, jens.e.bremnes@ntnu.no, asgeir.sorensen@ntnu.no).*

Abstract: Autonomous underwater vehicles (AUVs) rely on surface support for communication with operators and position fixes to bound inertial navigation errors. By installing an acoustic modem on an autonomous surface vehicle (ASV), the ASV can carry out these tasks, replacing more expensive and less flexible manned research vessels. This paper proposes a hybrid tracking controller for an ASV providing mission support for an AUV. The proposed controller keeps the ASV in a donut-shaped safety domain about the AUV defined by the risk of collision (inner boundary) and the risk of communication loss (outer boundary). At the same time, the hybrid controller reduces power consumption and acoustic signal noise by going into standby mode when it is within the safety domain. Results from a simulation study and field trials are presented to demonstrate and validate the controller's performance. The results show that the controller performed well in the tested cases.

Keywords: Unmanned marine vehicles, autonomous surface vehicles, autonomous underwater vehicles, coordinated control, hybrid dynamical systems, collision avoidance

1. INTRODUCTION

Recent years have seen large developments in field robotics, enabled by new and improved sensor, computer, communication, and navigation technologies. Reduced dependency on human operators leads to increased human safety and has proven to be cost-efficient and more environmentally friendly (Ventikos et al., 2020; Utne et al., 2020). The transition towards higher levels of autonomy is also underway in the marine industry, where agents with some degree of autonomy have gained significant traction (Ludvigsen and Sørensen, 2016). Two examples of such agents are autonomous surface vehicles (ASVs) and autonomous underwater vehicles (AUVs). ASVs are surface-going sensor-carrying platforms, while AUVs are sensor-carrying platforms with possibilities of under- and on-surface operation.

Some tasks are too complex for single agents to solve alone, and there is increased focus on combining multiple marine agents in robotic organizations. Robotic organizations can become powerful systems for mapping and monitoring the marine environment (Sørensen et al., 2020). One such system is an ASV aiding one or several AUVs in operation, replacing the manned support vessel that AUVs rely on. Taking the role as unmanned support vessels, ASVs can serve as communication hubs, relaying information between the AUV and the control center.

Without external aiding, AUVs rely on inertial navigation when submerged in water, leading to an unbounded error growth. External aiding can be provided by GPS on the surface or acoustic signals underwater (Ludvigsen and Sørensen, 2016). With ultra-short baseline (USBL) acoustic communication, a transducer mounted on an ASV can detect the range and bearing to an acoustic modem on the AUV, thus augmenting the inertial navigation error. USBL positioning is limited to the acoustic communication range, which depends largely on water conditions like salinity, temperature, and turbidity (Sørensen et al., 2020).

Several research groups have deployed teams of ASVs and AUVs under coordinated control. Fallon et al. (2010) and Norgren et al. (2015) propose control strategies where the ASV maintains a specified distance and bearing to an AUV. In these strategies, the ASV is constantly moving, leading to potentially excessive control action and propeller noise that affects the acoustic signals. On the other hand, Vasilijević et al. (2017) and Antonelli et al. (2018) propose control strategies where the ASV follows a pre-planned route chosen to stay sufficiently close to the AUV's planned route. For these strategies, successful missions thus depend on the AUV following its planned route; there is no room for autonomy. To allow for higher levels of autonomy, Willners et al. (2019) and Sture et al. (2020) propose cost-optimal controllers for an ASV aiding one or multiple AUVs. However, these controllers are complex and potentially challenging for operators to tune and use.

Building on previous work, this paper attempts to solve remaining challenges related to ASV control in ASV-AUV operations. In doing so, it evaluates two main research questions: Which risks emerge from combining an ASV with an AUV in a robotic organization? How can an ASV be used to provide mission support for an AUV while managing the emergent risks?

10.1016/j.ifacol.2022.10.414

The main scientific contribution of the present work is the development of a tracking controller for an ASV following an AUV. This is useful for aiding the AUV with USBL position fixes, as well as functioning as a communication gateway between the AUV and human operators. The tracking controller has collision avoidance properties and ensures communication between the vehicles is maintained, allowing the ASV to perform its gateway role while reducing risks. Moreover, formulating the control algorithm as a hybrid dynamical system represents another scientific contribution.

The paper is outlined as follows: Section 2 describes the system in more detail and presents the ASV tracking controller as a hybrid dynamical system, Section 3 introduces the experimental setup and discusses the results, while Section 4 concludes the paper and suggests areas of future work.

2. METHODOLOGY

2.1 Hybrid Dynamical Systems

The proposed tracking controller is modeled as a hybrid dynamical system based on the framework presented by Goebel et al. (2012). Such systems have both continuous-time and discrete-time dynamics, and their general model is expressed as

$$\mathcal{Q} = \begin{cases} \dot{x} \in \mathcal{F}(x) & \text{for } x \in \mathcal{C}, \\ x^+ \in \mathcal{G}(x) & \text{for } x \in \mathcal{D}, \end{cases} \tag{1}$$

where $\mathcal{C} \in \mathbb{R}^n$ is the flow set, $\mathcal{F} : \mathbb{R}^n \rightrightarrows \mathbb{R}^n$ is the flow map, $\mathcal{D} \in \mathbb{R}^n$ is the jump set, and $\mathcal{G} : \mathbb{R}^n \times \mathbb{R}^m \rightrightarrows \mathbb{R}^n$ is the jump map. The flow map $\mathcal{F}$ describes how the state x is allowed to change continuously when the state belongs to the flow set $\mathcal{C}$. Similarly, the jump map $\mathcal{G}$ describes how the state is allowed to change discretely when it belongs to the jump set $\mathcal{D}$.

The controller makes use of a simplified kinematic model for marine vessels described in detail in Fossen (2011). The kinematic relationship between velocities in the Earth-fixed ($\dot{\eta} \in \mathbb{R}^6$) and body-fixed ($\nu \in \mathbb{R}^6$) reference frames is expressed as

$$\dot{\eta} = \begin{bmatrix} J_1(\Theta) & 0_{3\times3} \\ 0_{3\times3} & J_2(\Theta) \end{bmatrix} \nu = J(\Theta)\nu, \tag{2}$$

where $J(\Theta) \in \mathbb{R}^{6\times6}$ is Euler angle transformation matrix. In this paper, the horizontal position component of η will be represented as $\xi = [N \;\; E]^T$, where N and E are North and East components, while ψ is the heading of the vessel relative to North. Subscript wp indicates the desired state defined by a waypoint.

2.2 Safety Domain

For the ASV to function as a communication link between the control center and the AUV, as well as supporting the AUV with navigation, USBL communication between the vehicles must be maintained. Loss of communication is a hazardous event that emerges when theses vehicles are combined in a robotic organization. To manage the corresponding emergent risk, the ASV must stay within a safety domain about the AUV where the outer boundary of the domain is defined by the USBL modem's maximum range.

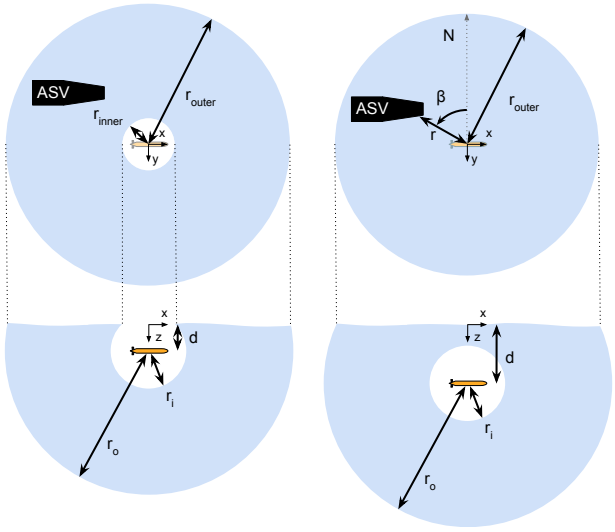

(a) $d < r_i$. (b) $d > r_i$.

Fig. 1. Safety domain for AUV at depth d. The bottom part of each subfigure illustrates the spheres around the AUV, while the top parts show their translations to the surface domain. For simplicity it is here assumed that the acoustic signal is not significantly affected by the surface.

There is often large variability in this range due to water conditions, with at times potentially sporadic USBL fixes. For these reasons, a safety factor α_{outer} is incorporated into the USBL modem's rated maximum range, r_0. Thus, the outer boundary of the safety domain is a sphere centered at the AUV with radius r_o defined as per

$$r_o = \frac{1}{\alpha_{outer}} r_0. \tag{3}$$

Another hazardous event that emerges with ASV-aided AUV operation is that of the ASV getting too close to the AUV, which can lead to inter-vehicle collision. To manage the emergent risk of this hazardous event, the ASV must maintain a minimum safety distance r_i to the AUV. Thus, the safety domain has an inner boundary defined by a sphere centered at the AUV with radius r_i.

To avoid collision in the worst-case scenario, this safety distance should be as large as the maximum expected displacement of the ASV relative to the AUV between two USBL fixes. Like the outer boundary, a safety factor α_{inner} is incorporated into the USBL update period, so the inner safety domain boundary is expressed as

$$r_i = \alpha_{inner} T_0 \dot{r}_{max}, \tag{4}$$

where T_0 is the rated USBL update period and $\dot{r}_{max}$ is the maximum relative speed between the ASV and the AUV. The safety factor incorporates uncertainty in the USBL update period and inertia in the ASV's dynamics. By choosing a sufficiently large α_{inner}, the risk of collision is kept low throughout the mission. Examples of appropriate values for α_{outer} and α_{inner} are shown in the case studies, Section 3.

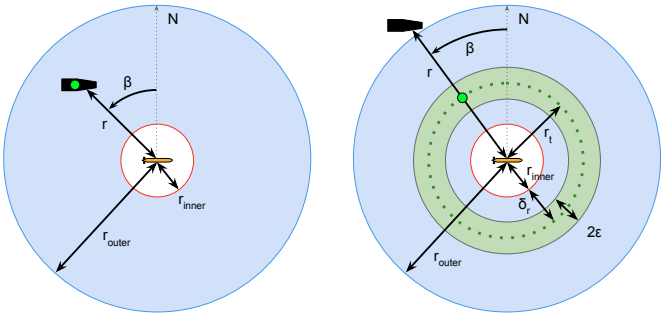

(a) Standby ($\mathcal{Q}_1$). The ASV is not using thrusters to reduce power consumption and acoustic noise from propeller.

(b) Transit ($\mathcal{Q}_2$). The ASV breaches safety domain and initiates transit towards or away from the AUV.

Fig. 2. Hybrid controller behavior. The green dots indicate ASV waypoints (WPs). When the ASV reaches the waypoint after transit, it goes back to standby mode. The dark green dotted circle is the target circle of radius $r_t = r_{inner} + \delta_r$ with the target domain indicated by the green donut around the target circle.

As seen in Fig. 1, the spheres about the AUV transform into a donut-shaped safety domain on the surface. The inner boundary of the donut is at distance r_{inner} from the AUV's position in the horizontal plane, while the outer boundary is at distance r_{outer}. For AUV depth d,

$$r_{inner} = \begin{cases} \sqrt{r_i^2 - d^2} & \text{for } d \leq r_i \\ 0 & \text{for } d > r_i \end{cases}$$
$$r_{outer} = \begin{cases} \sqrt{r_o^2 - d^2} & \text{for } d \leq r_o \\ 0 & \text{for } d > r_o \end{cases} \tag{5}$$

Note that if $d > r_i$, the safety domain is simply a circle because the inner boundary does not touch the surface, as shown in Fig. 1b. Similarly, if $d > r_o$, the safety domain is non-existent on the surface, so the AUV should not dive that deeply.

The radial distance (r) and bearing (β) from the AUV to the ASV are defined as

$$r = \sqrt{(N_{asv} - N_{auv})^2 + (E_{asv} - E_{auv})^2},$$
$$\beta = atan2\left(E_{asv} - E_{auv}, N_{asv} - N_{auv}\right). \tag{6}$$

2.3 Hybrid Controller

The objective of the controller is to keep the ASV within the safety domain. However, excessive ASV control action should also be avoided to improve performance and reduce power consumption. In addition, the noise of the ASV's propeller may significantly deteriorate acoustic signals. Therefore, the tracking controller is implemented as a hybrid controller capable of switching between a standby mode and a transit mode. The hybrid controller consists of a zero-thrust standby controller ($\mathcal{Q}_1$) and a set-point controller ($\mathcal{Q}_2$), and the controller behavior is presented graphically in Fig. 2.

$\mathcal{Q}_1$ is the preferred controller when the ASV is within the safety domain (Fig. 2a). To prevent unnecessary control action, the ASV is set to standby, meaning the thrusters are turned off while sensors remain on to monitor the operation.

If the ASV leaves the safety domain, however, control action is necessary. In this case, control is transferred to $\mathcal{Q}_2$, which updates the ASV's waypoint to the closest point on a target circle. This target circle, represented by the dark green line in Fig. 2, is expressed as

$$\xi_{wp,asv} = \xi_{auv} + r_t \begin{bmatrix} cos(\beta_{wp}) \\ sin(\beta_{wp}) \end{bmatrix}, \tag{7}$$

where β_{wp} is the bearing from the AUV towards the desired ASV position on the target circle. $\beta_{wp} = \beta$ represents the point on the target circle closest to the ASV. The radius of the target circle, r_t, is defined as

$$r_t = r_{inner} + \delta_r, \tag{8}$$

where δ_r is a tuning parameter that defines the horizontal margin from the safety domain's inner boundary to the target circle. When the ASV is tracking the AUV ($\mathcal{Q}_2$), a small δ_r means that the ASV moves closer to the AUV before changing to standby ($\mathcal{Q}_1$), which likely decreases the chance of leaving the outer boundary of the safety domain again. However, a small δ_r also comes with a higher risk of breaching the inner boundary.

To avoid high frequency switching between $\mathcal{Q}_1$ and $\mathcal{Q}_2$, the controller does not switch back from $\mathcal{Q}_2$ to $\mathcal{Q}_1$ until the ASV is sufficiently close to the target circle. This is quantified by the error, e, defined as

$$e = r - r_t, \tag{9}$$

which must be smaller than ε_- or ε_+, depending on the sign of e. This acceptable deviation from the target circle converts to the green target domain in Fig. 2, defined by

$$r \in [r_t - \varepsilon_-, r_t + \varepsilon_+], \tag{10}$$

where ε_- and ε_+ are tuning parameters. In this work, $\varepsilon_- = \varepsilon_+ =: \varepsilon$ is considered for simplicity. Differing values of ε_- and ε_+ can be considered in further studies. The controller accepts jumps to $\mathcal{Q}_1$ if the ASV is within the target domain.

As such, the proposed hybrid tracking controller based on the framework in (1) is formulated in (11) with subscripts 1 and 2 corresponding to $\mathcal{Q}_1$ and $\mathcal{Q}_2$, respectively. The controller state is $x = [r_{wp}, \beta_{wp}, r, \beta, q]^T$.

$$\mathcal{F}_1(x) := \begin{cases} \dot{r}_{wp} = \dot{r} \\ \dot{\beta}_{wp} = \dot{\beta} \\ \dot{q} = 0 \end{cases} \quad \text{for } x \in \mathcal{C}_1 := \{x : q = 1\}$$
$$\mathcal{G}_1(x) := \begin{cases} r_{wp}^+ = r \\ \beta_{wp}^+ = \beta \\ q^+ = 1 \end{cases} \quad \text{for } x \in \mathcal{D}_1 := \left\{ \begin{matrix} x : |e| < \varepsilon, \\ q = 2 \end{matrix} \right\}$$
$$\mathcal{F}_2(x) := \begin{cases} \dot{r}_{wp} = \dot{r}_t \\ \dot{\beta}_{wp} = \dot{\beta} \\ \dot{q} = 0 \end{cases} \quad \text{for } x \in \mathcal{C}_2 := \{x : q = 2\}$$
$$\mathcal{G}_2(x) := \begin{cases} r_{wp}^+ = r_t \\ \beta_{wp}^+ = \beta \\ q^+ = 2 \end{cases} \quad \text{for } x \in \mathcal{D}_2 := \{x : r \notin [r_{inner}, r_{outer}]\} \tag{11}$$

Once the appropriate controller has been selected in (11), the ASV waypoint is updated as per (7).

The proposed tracking algorithm relies on knowledge of the AUV's navigational states. However, the USBL communication link only provides this information sporadically. Thus, the ASV must be capable of estimating the AUV's navigational states between updates.

3. RESULTS AND DISCUSSION

3.1 Experimental Setup

To demonstrate and validate the performance of the controller, a simulation study was conducted, followed by field trials with a physical ASV and a simulated AUV.

The ASV used in the present work is a Pioner 17 from Maritime Robotics named Gretha, while the AUV is a simulated AUV modeled after a light AUV (LAUV) from OceanScan named Fridtjof.

Gretha is 5.2 m long, 2.15 m wide, has a draft of 0.3 m and weighs 810 kg. While the vehicle's rated top speed is 6 kn, its rated endurance is 24 hours at 3 kn. The on-board communication suite consists of a WiFi hotspot with more than 50 m range, LTE coverage through a 4G module, and Kongsberg MBR broadband with 15 km range. Additionally, an EvoLogics S2C R 18/34 USBL modem with range $r_0 = 3.5$ km was installed to facilitate acoustic communication with the AUV.

Fridtjof is 1.80 m long, has a diameter of 20cm and weighs 25.8 kg. The vehicle's maximum speed is 2 m/s, and the rated endurance is 8 hours at maximum speed. Fridtjof's on-board communication suite consists of a WiFi antenna with 1 km range, GSM coverage through a 3G module, and an Iridium SBD module with global coverage, as well as an underwater acoustic modem. Only the latter is used when the AUV is submerged, as the former three technologies only work in air.

When the AUV is on the surface and sufficiently close to the ASV, the vehicles communicate real-time via WiFi. When the AUV is submerged, however, they rely on the acoustic link for underwater communication. USBL position fixes are typically available every $T_0 = 5$ s, meaning communication is often limited. Moreover, experience shows that despite the 3.5 km rated range, the signal is good only up to about 500-1000 m, depending on the water conditions. It is not uncommon that signals are not properly received, especially if the distance between the acoustic modems is large or water characteristics such as salinity and turbidity are varying.

The main software used for both simulations and field trials is the LSTS toolchain. This toolchain consists of DUNE on-board software, [1] Neptus command and control software, [2] and the IMC communications protocol. [3] Fridtjof is simulated in DUNE with a standard LAUV simulator, while Gretha comes with Maritime Robotics's in-house Onboard System (OBS) for control, navigation, and communication. Their graphical user interface for command and control, which has a built-in simulator for Gretha, is called Vehicle Control Station (VCS). To integrate OBS/VCS with the LSTS toolchain, a software bridge between the two interfaces was designed. The controller was implemented with Python in ROS, [4] so another software bridge was set up between IMC and ROS based on the *imc_ros_bridge* package. [5]

In the simulation study, two cases of typical AUV operation (Case 1 and Case 2) were simulated using the default LAUV simulator in DUNE, as well as the Gretha simulator in VCS. In Case 1, the AUV first does overview scans of two areas before performing closer inspection of detected areas of interest. In Case 2, the AUV continues to another area to do a third overview scan instead of performing closer inspection. AUVs normally operate on altitude control during seabed surveys, but without loss of generality, depth control is used in these test cases for simplicity. The hybrid tracking controller's performance was analyzed by running it on the ASV and studying the vehicle's resulting behavior.

After the controller was validated in numerical simulations, field trials were conducted in the Trondheimfjord in April and May 2022 with Gretha and a simulated AUV.

In Case 3, the ASV and AUV both start some distance from the operational area, which consists of a stretched-out lawnmower pattern. The length of the pattern is larger than in the simulation cases to showcase the ASV's tracking abilities. Rather than a constant altitude control law, the simulated AUV operates in the surface with a zero-depth set-point during the test to better illustrate the controller's behavior. This gives a worst-case condition with respect to the size of the anti-collision domain.

In Case 4, the AUV actively tries to breach the inner boundary, to generate challenging scenarios, by moving in an unpredictable manner, often straight towards the ASV. In essence, the AUV behaves as an adversary or a pursuer. Although this behavior is unlikely during nominal operation, it is difficult to predict how an autonomous vehicle will behave, for instance if it follows an adaptive sampling control law. Therefore, Case 4 is mainly focused on how the hybrid tracking controller prevents possibly dangerous situations when the AUV operates with high levels of autonomy. Like in Case 3, the AUV remains on the surface in Case 4.

Since the AUVs are simulated, the ASV has continuous knowledge of their navigational states. During operations with physical AUVs, it is assumed that continuous knowledge of AUVs' navigational states is made possible with a state estimator. This is out of scope of this paper and is thus not implemented here.

The testing cases for the field trials are simpler than those used in simulation because of the unpredictable and unforgiving environment of the ocean. Therefore, results from simulations and field trials are intended to complement each other.

3.2 Tuning Parameters

Several tests were run to determine suitable values for the tuning parameters. The values chosen for simulations were modified during field trials to achieve better performance.

[1] https://github.com/LSTS/dune
[2] https://github.com/LSTS/neptus
[3] https://lsts.pt/docs/imc/master/index.html
[4] https://www.ros.org
[5] https://github.com/smarc-project/imc_ros_bridge

Table 1 summarizes the numerical values, and the text below justifies the selection.

Table 1: Tuning Parameters.

Parameter	Simulations	Field Trials
α_{outer}	11.7	17.5
α_{inner}	5	5
δ_r	125 m	20 m
ε	30 m	10 m

The selection of domain-defining tuning parameters for simulations was based on a priori knowledge of the system. Firstly, the inner boundary safety factor was set to $\alpha_{inner} = 3$, yielding an inner boundary of the safety domain ($r_{inner} = 30$ m), which prevented collision in the worst-case scenario. Secondly, the outer boundary safety factor was set to $\alpha_{outer} = 11.7$, yielding $r_{outer} = 300$ m, which maintained reliable and accurate USBL fixes throughout the safety domain, while minimizing control action and consequently propeller usage. Thirdly, the margin from r_{inner} to the target circle was set to $\delta_r = 125$ m, to achieve a target circle that was approximately in the middle of the safety domain. Lastly, the acceptable distance to the target circle before changing to standby mode was set to $\varepsilon = 30$ m.

While yielding promising results in the simulations, the tuning parameters had to be adjusted during field trials for improved performance. Since the dynamics of the ASV were found to be much slower than those of the ASV simulator used during simulation-based testing, the inner boundary of the safety domain was increased with $\alpha_{inner} = 5$, giving $r_{inner} = 50$ m. Moreover, since the ASV was significantly slower than its rated top speed ($u_{max,test} = 4.9$ kn vs. $u_{max,rated} = 6$ kn), the safety factor for the safety domain's outer boundary had to be increased to $\alpha_{outer} = 17.5$, giving $r_{outer} = 200$ m. This was for the ASV to quickly reach the target circle during tracking, even with the AUV moving away from the ASV. For the ASV to remain closer to the AUV, the margin from r_{inner} to the target circle was reduced to $\delta_r = 20$ m, giving a target circle radius r_t ranging from 20 m if the AUV is deeply submerged to 70 m if the AUV is on the surface. The acceptable distance to the target circle before jumping to standby mode was reduced to $\varepsilon = 10$ m to make a smaller target domain, appropriate for a target circle closer to the safety domain's inner boundary.

3.3 Discussion

Fig. 3 shows how, despite the AUV's large operational area, the ASV does not move much in simulated Case 1. While the AUV travels 4.25 km, the ASV moves less than 620 m during the entire simulation, which is only 15% of the AUV's traveled distance. Moreover, the ASV is in standby mode for 2891 s (89% of simulation), while it is in transit mode for only 357 s (11% of simulation, 28 s collision avoidance, 329 s tracking). This is largely because each overview scan is small enough that the ASV stays mostly within the safety domain. Such behavior is beneficial because it reduces wear and tear on the propulsion system, lowers energy usage, and improves the acoustic environment. Fig. 4 helps explain how the ASV can stay mostly stationary in standby mode. Until $t =$

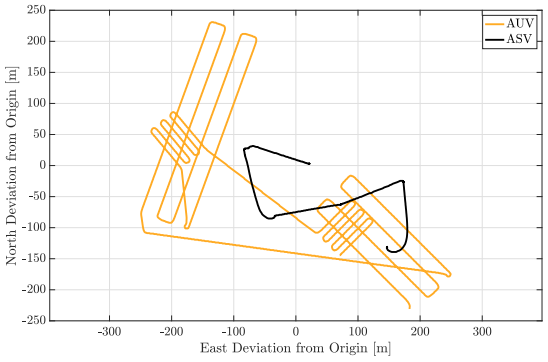

Fig. 3. Case 1: North and East movement of the two vehicles relative to the origin, defined as the center point of the operation.

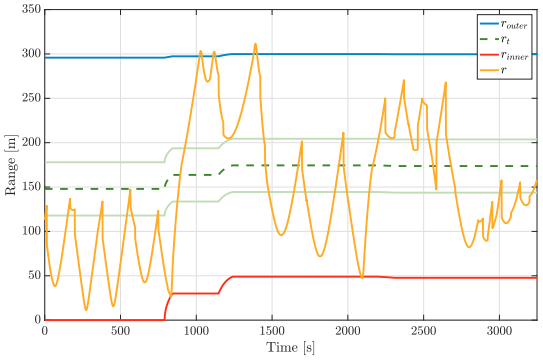

Fig. 4. Case 1: Time development of the range between the ASV and the AUV (r) compared to the radii of the outer safety boundary (r_{outer}), the target circle (r_t) surrounded by the target domain boundaries in lighter green, and the inner boundary (r_{inner}).

835 s, the ASV is drifting in the middle of the AUV's lawnmower path, with the AUV sufficiently submerged that collision avoidance is not necessary. However, when the AUV transits to the Western part of its operational area, collision avoidance is initiated as the ASV breaches the inner boundary at $t = 835$ s, before tracking is initiated when the ASV breaches the outer boundary at $t = 1022$ s and again at $t = 1378$ s. One more collision avoidance is required at $t = 2095$ s, but apart from that the ASV is in standby mode.

Since the AUV transits to a different area for the third overview scan, the ASV has to move further in Case 2, as seen in Fig. 5. The AUV moves 4.99 km, while the ASV travels 1.19 km during the 1-hour simulation. Although the ASV does more tracking than in Case 1, the total distance traveled is still only 24% of that of the AUV, confirming that the ASV moves conservatively. This is validated by Fig. 6, which shows the ASV-AUV range compared to the boundaries of the safety domain. For most of the operation, the ASV is drifting within the safety domain; it spends 3115 s (81%) in standby mode and only 714 s (19%) in transit mode (680 s tracking and 34 s collision avoidance). Tracking is initiated at $t = 1240$ s, 2325 s, and 2930 s, and collision avoidance at $t = 2150$ s, and 3200 s, but the ASV quickly moves to the target domain to re-enter standby mode every time.

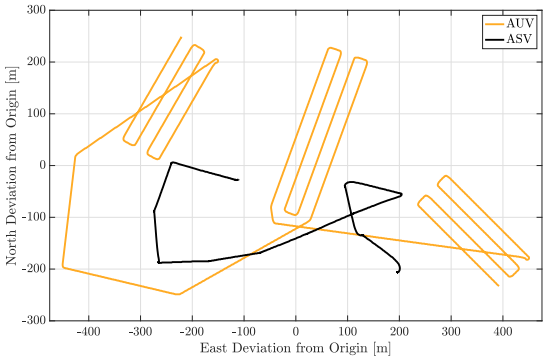

Fig. 5. Case 2: North and East movement of the two vehicles relative to the origin, defined as the center point of the operation.

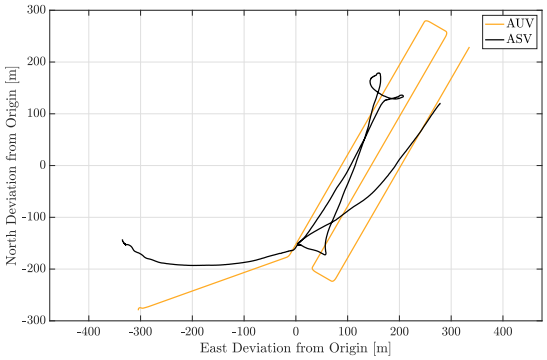

Fig. 7. Case 3: North and East movement of the two vehicles relative to the origin, defined as the center point of the operation.

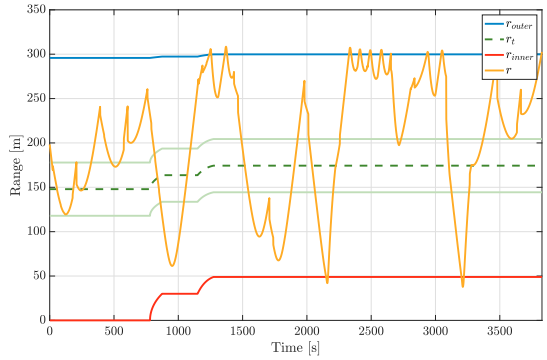

Fig. 6. Case 2: Time development of the range between the ASV and the AUV (r) compared to the radii of the outer safety boundary (r_{outer}), the target circle (r_t) surrounded by the target domain boundaries in lighter green, and the inner boundary (r_{inner}).

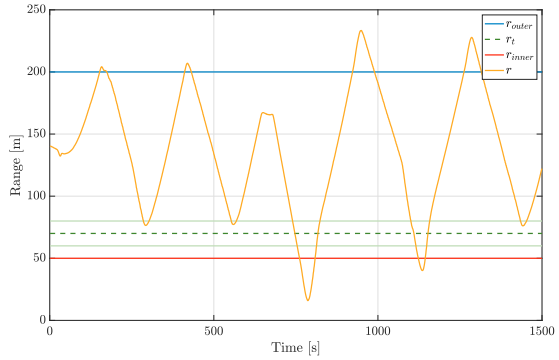

Fig. 8. Case 3: Time development of the range between the ASV and the AUV (r) compared to the radii of the outer safety boundary (r_{outer}), the target circle (r_t) surrounded by the target domain boundaries in lighter green, and the inner boundary (r_{inner}).

Like in Case 1, Case 2 shows that the hybrid tracking controller maintains a low risk of both collision and loss of communication, while not using excessive control. The ability to move autonomously without prior knowledge of the AUV's planned route makes the controller applicable to a range of operational types.

Moving onto the results from field trials, the North and East movement of both vehicles during Case 3 is presented in Fig. 7. Like in the simulated cases, the ASV travels significantly shorter than the AUV by not following the underwater vehicle to the extremities of the operation. The total distance traveled by the AUV in Case 3 is 1.98 km, while the ASV travels 1.68 km, or 85% of that of the AUV.

Fig. 8 explains the ASV's movement in Case 3 in more detail. Corrective action is taken quickly when the AUV breaches the safety domain, thus initiating a collision avoidance maneuver, which limits the range to the interval $r \in [17\text{ m}, 233\text{ m}]$. The ASV maintains safe operation without excessive control action, as verified by the total time spent in each operation: 798 s (53%) in standby mode and 702 s (47%) in transit mode (633 s tracking and 69 s collision avoidance). The portion spent in transit is larger than for the simulated cases because of the layout of the AUV's operational area, and since the outer boundary of the safety domain was reduced to 200 m, with the target circle closer to the inner boundary.

As for Case 4, Fig. 9 shows how the ASV repeatedly breaches the safety domain's inner boundary, each time initiating a collision avoidance maneuver. Even with the AUV moving straight towards the ASV at maximum speed, it was not possible to obtain a range smaller than $r = 15.5$ m at any point during the test. This verifies the ASV's collision avoidance properties. Like in Case 3, the corrective action in Case 4 is also efficient, with only 409 s (33%) spent in transit mode (232 s tracking and 177 s collision avoidance), compared to 833 s (67%) in standby mode.

For closer inspection of the behavior seen in Fig. 9, four snapshots of the vehicles during the collision avoidance period $t \in [\,98\text{ s}, 235\text{ s}]$ are presented in Fig. 10. The first snapshot (Fig. 10a) shows the ASV in collision avoidance at $t = 120$ s. As seen in Fig. 9, the ASV reaches the target domain and enters standby mode at $t = 88$ s. Because of the ASV's inertia, the vehicle is still drifting towards the AUV when collision avoidance is initiated at $t = 98$ s. Thus, it takes another 22 s until the ASV has turned around and started moving away from the AUV at $t = 120$ s, reaching the minimum range $r = 15.5$ m.

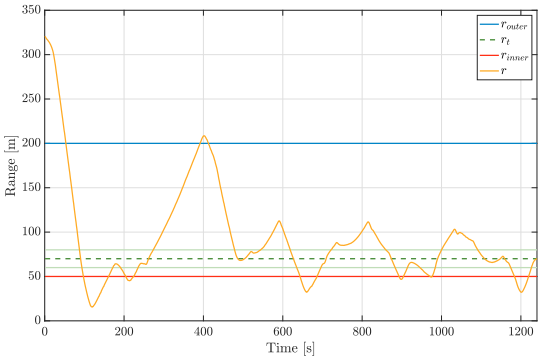

Fig. 9. Case 4: Time development of the range between the ASV and the AUV (r) compared to the radii of the outer safety boundary (r_{outer}), the target circle (r_t) surrounded by the target domain boundaries in lighter green, and the inner boundary (r_{inner}).

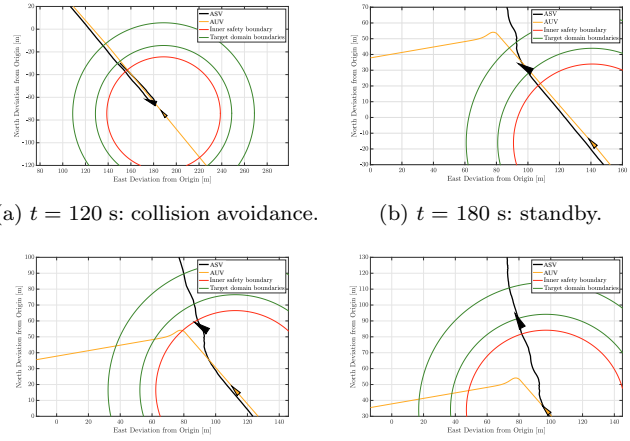

(a) $t = 120$ s: collision avoidance. (b) $t = 180$ s: standby.

(c) $t = 215$ s: collision avoidance. (d) $t = 235$ s: standby.

Fig. 10. Case 4: Snapshots of position and heading for the ASV and the AUV during collision avoidance. The red circles indicate the anti-collision domain around each AUV, while the green circles symbolize the boundaries of the target domain.

The ASV then quickly moves away from the AUV and reaches the target domain at $t = 180$ s to enter standby mode (Fig. 10b). Since the AUV is still moving the same direction, the ASV breaches the inner boundary again at $t = 215$ s (Fig. 10c), but since the ASV is now stationary and its heading is already close to the desired heading, it only takes 20 s before the ASV reaches the target domain again at $t = 235$ s (Fig. 10d). After this, the AUV changes heading, meaning the ASV can stay in standby mode until tracking is initiated at $t = 395$ s, as seen in Fig. 9.

4. CONCLUSION

The proposed hybrid tracking controller for an ASV aiding and supporting an AUV is a simple but flexible controller. While reducing the emergent risks of acoustic communication loss and inter-vehicle collision, the controller prevents excess thruster usage with a standby control mode. Three controller tuning parameters, α_{outer}, α_{inner}, and ε, can be modified to obtain desired behavior. The controller performed well in simulation, and field trials further validated its performance. Areas of future work include a more comprehensive evaluation of emergent risks, and dynamic selection of tuning parameters.

ACKNOWLEDGEMENTS

This work was supported by the Research Council of Norway through the Centre of Excellence funding scheme, NTNU AMOS, project number 223254, NTNU VISTA CAROS, and the UNLOCK project, through the Research Council of Norway FRINATEK scheme, project number 274441. We would also like to thank AUR-Lab for their valuable input. The comments by two anonymous reviewers are highly appreciated for improving this article.

REFERENCES

Antonelli, G., Arrichiello, F., Caiti, A., Casalino, G., Palma, D.D., Indiveri, G., Razzanelli, M., Pollini, L., and Simetti, E. (2018). ISME activity on the use of autonomous surface and underwater vehicles for acoustic surveys at sea. *ACTA IMEKO*, 7, 24–31.

Fallon, M., Papadopoulos, G., Leonard, J., and Patrikalakis, N. (2010). Cooperative AUV navigation using a single maneuvering surface craft. *International Journal of Robotics Research*, 29, 1461–1474.

Fossen, T. (2011). *Handbook of Marine Craft Hydrodynamics and Motion Control*. John Wiley & Sons.

Goebel, R., Sanfelice, R.G., and Teel, A. (2012). *Hybrid dynamical systems: Modeling, stability, and robustness*. Princeton University Press.

Ludvigsen, M. and Sørensen, A. (2016). Towards integrated autonomous underwater operations for ocean mapping and monitoring. *Annual Reviews in Control*, 42, 145–157.

Norgren, P., Ludvigsen, M., Ingebregtsen, T., and Hovstein, V. (2015). Tracking and remote monitoring of an autonomous underwater vehicle using an unmanned surface vehicle in the Trondheim fjord. *OCEANS 2015 - MTS/IEEE Washington*.

Sture, Ø., Norgren, P., and Ludvigsen, M. (2020). Trajectory planning for navigation aiding of autonomous underwater vehicles. *IEEE Access*, 8, 116586–116604.

Sørensen, A., Ludvigsen, M., Norgren, P., Ødegård, Ø., and Cottier, F. (2020). *POLAR NIGHT Marine Ecology*, chapter 9, 241–275. Springer.

Utne, I.B., Rokseth, B., Sørensen, A.J., and Vinnem, J.E. (2020). Towards supervisory risk control of autonomous ships. *Reliability Engineering and System Safety*, 196.

Vasilijević, A., Nad, D., Mandić, F., Mišković, N., and Vukić, Z. (2017). Coordinated navigation of surface and underwater marine robotic vehicles for ocean sampling and environmental monitoring. *IEEE/ASME Transactions on Mechatronics*, 22, 1174–1184.

Ventikos, N.P., Chmurski, A., and Louzis, K. (2020). A systems-based application for autonomous vessels safety: Hazard identification as a function of increasing autonomy levels. *Safety Science*, 131.

Willners, J., Toohey, L., and Petillot, Y. (2019). Sampling-based path planning for cooperative autonomous maritime vehicles to reduce uncertainty in range-only localization. *IEEE Robotics and Automation Letters*, 4, 3987–3994.